Title

Relative impact of uniaxial alignment vs. form-induced stress on differentiation of human adipose derived stem cells

Permalink

https://escholarship.org/uc/item/5d4483hg

Journal

Biomaterials, 34(38)

ISSN

0267-6605

Authors

Qu, Xin
Zhu, Wei
Huang, Samuel
et al.

Publication Date

2013-12-01

DOI

10.1016/j.biomaterials.2013.09.009

Peer reviewed

Relative impact of uniaxial alignment vs. form-induced stress on differentiation of human adipose derived stem cells

Xin Qu[#a], **Wei Zhu**[#a], **Samuel Huang**[b], **Julie Yi-Shuan Li**[b], **Shu Chien**[b], **Kang Zhang**[c], and **Shaochen Chen**[a,*]

[a]Department of NanoEngineering, University of California, San Diego, La Jolla, CA 92093

[b]Department of Bioengineering, University of California, San Diego, La Jolla, CA 92093

[c]Shiley Eye Center and Institute for Genomic Medicine, University of California, San Diego, La Jolla, CA 92093

[#] These authors contributed equally to this work.

Abstract

ADSCs are a great cell source for tissue engineering and regenerative medicine. However, the development of methods to appropriately manipulate these cells *in vitro* remains a challenge. Here the proliferation and differentiation of ADSCs on microfabricated surfaces with varying geometries were investigated. To create the patterned substrates, a maskless biofabrication method was developed based on dynamic optical projection stereolithography. Proliferation and early differentiation of ADSCs were compared across three distinct multicellular patterns, namely stripes (ST), symmetric fork (SF), and asymmetric fork (AF). The ST pattern was designed for uniaxial cell alignment while the SF and AF pattern were designed with altered cell directionality to different extents. The SF and AF patterns generated similar levels of regional peak stress, which were both significantly higher than those within the ST pattern. No significant difference in ADSC proliferation was observed among the three patterns. In comparison to the ST pattern, higher peak stress levels of the SF and AF patterns were associated with up-regulation of the chondrogenic and osteogenic markers SOX9 and RUNX2. Interestingly, uniaxial cell alignment in the ST pattern seemed to increase the expression of SM22 and smooth muscle -actin, suggesting an early smooth muscle lineage progression. These results indicate that geometric cues that promote uniaxial alignment might be more potent for myogenesis than those with increased peak stress. Overall, the use of these patterned geometric cues for modulating cell alignment and form-induced stress can serve as a powerful and versatile technique towards controlling differentiation in ADSCs.

Keywords

Adipose derived stem cells; Multicellular forms; Alignment; Form-induced stress; Differentiation

*Corresponding author. Department of NanoEngineering, SME Building, MC-0448, University of California, San Diego, 9500 Gilman Drive, La Jolla, CA 92093-0448 shc064@eng.ucsd.edu.

Introduction

Over the past decades, significant advances in tissue engineering have led to numerous promising approaches and potential therapies for regenerative medicine [1]. The use of stem cells has become a cornerstone in myriad tissue engineering applications, and the rapid development of methods for sourcing stem cells has largely aided this progress. In particular, adipose-derived stem cells (ADSCs), due to their differentiation potential and the relative ease and abundance with which they can be sourced, have attracted much attention within the field. ADSCs can differentiate into a variety of cell lineages, such as smooth muscle cells, chondrocytes, osteoblasts, and neurons [2–9]. Given the powerful utility of ADSCs, the development of methods for appropriately manipulating these cells *in vitro* – and eventually *in vivo* – is pivotal to their adoption in tissue engineering applications. In this work, we studied the differentiation of ADSCs on microfabricated surfaces that feature various geometric patterns to modulate cell alignment and thereby induce different cellular stresses.

Most studies investigating the cellular response of ADSCs to external cues have focused on the use of biochemical signals. However, mechanotransduction events involving cell-cell and cell-material interactions can play a significant role in directing cell activity and fate [10, 11]. For instance, Engler et al. used polyacrylamide gels to show that variations in substrate stiffness can induce MSC differentiation towards corresponding cell lineages [12]. The C. S. Chen group demonstrated that endothelial cells can form proliferation patterns that correspond to the internal stresses provided by various geometries designed to direct cell adhesion [13]. They also showed that – in comparison to MSCs that exhibit spheroid morphology – MSCs with a confined cell growth area up-regulate the expression of chondrogenic markers, whereas myogenesis was enhanced with normally spread morphology [14]. Furthermore, independent of soluble factors, osteogenesis was promoted in MSCs cultured on substrates with geometric cues designed to enhance cellular contractility [15]. Others have demonstrated that the expression of muscle-specific genes can be induced in stem cells by multicellular forms that promote uniaxial cell alignment [16]. Interestingly, a recent study by Munoz-Pinto et al. suggested that uniaxial alignment can induce more myogenesis in multipotent mouse stem cells than those with increased cell-substrate stress [17]. However, despite the demonstrated influence that mechanical and geometric cues can have on directing cell fate, to the best of our knowledge the number of studies that have translated these findings to ADSCs has been limited.

Recently, our group developed a mask-free microfabrication method based on dynamic optical projection stereolithography (DOPsL) [18]. Compared to other widely used patterning methods, such as micro-contact printing and conventional lithographic approaches, our system provides greater flexibility in direct printing 3-diemnsional (3D) structures and better biocompatibility for biological materials [18–20]. In this work, we utilized this DOPsL platform to create three designed multicellular forms and further studied the early stage differentiation of ADSCs on microfabricated surfaces to determine the relative impact of uniaxial cell alignment versus form-induced stress.

Material and Methods

Scaffold fabrication

Poly(ethyleneglycol) diacrylate (PEGDA, Mn = 700), 2,2,6,6-tetramethylpiperidine 1-oxyl (TEMPO, free-radical quencher) and 2-Hydroxy-4-methoxy-benzophenon-5-sulfonic acid (HMBS) were purchased from Sigma-Aldrich. Lithium phenyl-2,4,6-trimethylbenzoylphosphinate (LAP) photoinitiator was prepared as previously described [21]. Pre-polymer solution was prepared as follows. PEGDA (20 wt% Mn 700, Sigma-

Aldrich) was mixed with PBS, LAP (1 wt%) and Tempo (0.01 wt%). The mixture was vortexed (5 min) and sterilized by using a 0.22-μm pore size syringe filter. The PEGDA solution was sandwiched between a methacrylated coverslip and a glass slide holder with a PDMS spacer (50μm height). Samples were fabricated by 4 seconds of UV-light (365nm) exposure using the DOPsL biofabrication system (Fig. 1a) [18].

Cell Cultures

ADSCs were purchased from Lonza and cultured according to the protocol provided by the vendor using ADSC™ Growth Media BulletKit™ (Lonza). All experiments were carried out using ADSCs from passages 2 to 5. The cells were harvested and counted based on the general protocol and then seeded onto the scaffold with growth media. Media were initially changed one day after seeding and then refreshed every other day. To assess cell differentiation, the cultures were maintained for 7 days in a 37°C incubator with 5% CO_2.

Immunofluorescent staining

Cells were fixed after 7 days of culture and stained for differentiation markers and nuclei. 4% paraformaldehyde (Electron Microscopy Sciences) was used to fix the cells on the scaffold for 30 minutes at room temperature, and followed by permeabilization with 0.1% Triton X-100 (Sigma Aldrich) in PBS with 2% bovine serum album (BSA, Fisher Scientific) for 60 minutes. The cells were then exposed to 1:100 diluted primary antibodies (smooth muscle a-actin, Novus Bio; SM22, Santa Cruz; Runx2, Abnova, Sox9, Sigma; PPAR, Cell Signaling) at 4°C overnight. Secondary antibodies with fluorescent labels (goat anti mouse-DyLight 488, JacksonImmuno; goat anti rabbit IgG-CF594, Biotium) were applied to samples for 1 hour at room temperature. Nuclei were counterstained with Horchest 33258 DNA dye (Invitrogen). Fluorescent images were taken on Leica DMI 6000-B Microscope.

Finite element modeling of form-induced stress

The cell-substrate stress distributions induced by the three different patterns were modeled using COMSOL Multiphysics according to previously reported model [13, 17]. In brief, a three-dimensional finite-element model of the cell-substrate interaction was constructed with a contractile layer and a passive layer using previously reported physical parameters. The cell layer was represented by the contractile layer with a height of 20μm, a Young's modulus of 500Pa, a Poisson's ratio of 0.499, a thermal conductivity of $10Wm^{-1}K^{-1}$ and a coefficient of expansion of $0.05K^{-1}$. The passive layer was intended to represent the pendant protein chains adsorbed onto the substrate with a height of 4μm, a Young's modulus of 100Pa, and a Poisson's ratio of 0.499 [13, 17]. Since the surface of the substrate is very rigid, the bottom of the passive layer was treated as fixed constraint. In all simulations, a mesh of free tetrahedral was built with element sizes of 2–5μm. To simulate the monolayer cell contraction, a thermal strain was induced by a temperature drop of 5°K. The maximum principal stress at the fixed bottom surface was determined. Convergence of results was confirmed by varying the element sizes of the mesh and physical parameters.

qRT-PCR

ADSCs were seeded onto the patterned surfaces at $20,000/cm^2$ and maintained for 7 days in normal growth media before RNA extraction. Total RNA was isolated using TRIzol® (Invitrogen) with a manufacturer-suggested protocol. The concentration and quality of RNA were examined by using a Nanodrop spectrophotometer (Thermo). Reverse transcription of mRNA was carried out with 1 μg of total RNA using the MLV reverse transcriptase (Invitrogen) and oligo-dT primer at 42°C for 1 h. The synthesized cDNA was then used to perform quantitative real-time PCR (qRT-PCR) with the iQ SYBR Green supermix (Bio-

Rad) on the iCycler real-time PCR detection system (Bio-Rad). The primer sequences will be provided upon request.

Statistical Analysis

Data are reported as mean ± standard deviation. Comparison of sample means was performed by ANOVA followed by Tukey's post-hoc test (SPSS software), $p < 0.05$ was considered statistically significant.

Results and Discussion

Scaffold design and characterization

In the present study, three distinct patterns were designed and fabricated using the DOPsL platform, namely the stripe pattern (ST, Fig. 1b), symmetric fork pattern (SF, Fig. 1c) and asymmetric fork pattern (AF, Fig. 1d). Due to the high flexibility and the "mask-less" feature of the DOPsL system, several different parameters can be tested and optimized in an efficient manner. For instance, the pixel numbers of patterned area and gaps in the digital masks were optimized to form designed pattern without disrupting the gaps due to bleeding. All scaffolds were fabricated using 20% PEGDA without any cell adhesion ligand. Therefore, the fabricated wall-like structures were resistant to cell adhesion and could simply serve as obstructions to block cell spreading and migration. The height of the scaffold was controlled by the spacers, and all scaffolds had a height of approximately 50μm, which was sufficient to prevent cells from climbing over the walls. The gaps between the parallel walls were consistent across different scaffolds, being 177.4±2.9, 174.0±2.3, and 175.8±2.0μm in the ST, SF, and AF patterns, respectively (Fig. 1b–d). The gap between the spikes of the SF pattern was 105.6±4.0μm, and the gaps between the spikes of the AF pattern were 169.2±5.9 and 39.2±5.7μm. The gaps between the spikes and parallel wall were 57.4±4.0μm in the SF pattern, and 53.6±3.3μm in the AF pattern. The average widths of the walls were comparable across the patterns, being 21.1±0.7, 23.0±0.9, and 22.1±0.9μm for ST, SF, and AF patterns, respectively (Fig. 1b–d). With a single UV exposure, a typical patterned area in the DOPsL system is about 2mm by 3.5mm. However, this size is scalable for larger patterns through the precise motion of the sample stage and control of the DOPsL software. Due to the usage of highly efficient photoinitiator LAP, 4 seconds of UV exposure was sufficient for one single patterning, which added up to about 1 minute for a 3×3 tiled multi-patterning experiment. To further test the resolution limit, we also tried 1 pixel digital masks and 20% PEGDA, and these gave arise to scaffolds with feature sizes around 10 microns (Fig. S1). This resolution can be further improved to reach a sub-micron scale when a lens of higher numerical aperture is used.

Assessment of cell alignment

Human adipose-derived stem cells were cultured and seeded on to the patterned surfaces, and the cell alignment was monitored. Hoechst staining was used to stain the nuclei and later used for quantitative analysis of cell alignment. The fluorescent images of F-actin showed that the cells followed the walls created in the device and formed multicellular forms by design (Fig. 2c). In order to further quantify the cell alignment, the nuclear staining was subjected to an automated image analysis method [22] (Fig. 2b). In brief, the nuclear staining images were binarized and imported into MATLAB, and the orientations of the nuclei were profiled using an in-house developed algorithm. All readings from multiple independent pictures (n>10) were pooled to generate the histogram in Fig. 2a. The cells in the ST pattern showed one strong peak around zero degree (Fig. 2a, black curve), indicating that cell alignment is primarily along the same direction as the PEG walls. In the SF and AF patterns, the spikes between the stripes were designed to interrupt cell alignment. The cells in the SF pattern showed a significantly depressed peak at zero degree and two symmetric

peaks on the shoulders (Fig. 2a, red curve). In the AF pattern, the main peak at zero degree remained similar to that in SF, but there is also a very wide peak next to it (Fig. 2a blue curve), indicating a more random cellular directionality. The nuclear staining is a good approach to assess the cell alignment since it is a convenient mark to isolate individual cells, although it may slightly increase the noise because the shape of the nuclei is less asymmetrical than the cell. Although cytoskeletal staining (e.g., F-actin) could be another option [22], the overlapping of actin filaments due to the high cell density in our experiments (Fig. 2c) made it very challenging to isolate individual cells for the analysis of cell directionality. The alignment histogram demonstrates that our microfabricated surfaces could guide ADSCs to form multicellular forms by design and that the cellular alignment was interrupted in the SF pattern and further impaired in the AF pattern.

Evaluation of relative stresses within the patterns

Finite element simulation was performed to evaluate the relative stresses within the multicellular forms. In all three patterns, the contraction of the cellular sheet induced a higher traction stress on the edges than the interior part, and a maximum stress was observed in AF and SF at the corners where spikes and parallel walls joined. (Fig. 3a). The AF and SF designs changed the distribution of the relative stresses compared to those in the ST design, and the results showed that SF and AF patterns experienced a higher traction stresses along the patterned spikes. To further elucidate the difference of relative stresses in the three patterns, a distribution histogram was generated using the data across the patterns horizontally in the center (Fig. 3b). The maximum relative stress at the spike edges of the AF and SF patterns can be nearly 3 times as high as the stress in the interior part of all three patterns. The closer to the edge, the higher was the relative stress. For the ST pattern, since there are no interior edges, the stress is evenly distributed (Fig. 3b, black line). To further validate the relative stress pattern, heat maps were generated as previously described using F-actin staining [13]. As shown in Fig. 3c, cell distribution was homogenous in the ST pattern, whereas in the AF and SF patterns, more cells were localized towards the center of the pattern and away from the edges. Due to the resistance of cell adhesion to the PEGDA walls, the cells near the edge could be potentially pulled by cells located in the center of the patterns and thus formed the final multicellular forms. This is consistent with the simulation results, in which higher relative stress emerges towards the edges, and more cellular deformation is to be expected [23]. Further investigation of cell proliferation was carried out using EdU assay (Invitrogen) showed limited effect of these patterns on ADSC proliferation (Fig. 4). These results suggest that the formation of these multicellular forms could be mainly due to the re-organization of cell distribution rather than the emergent patterns of cell growth. This observation seems contradictory to the findings in endothelia cells cultivated on patterned surfaces, where cell-substrate stresses can induce patterns of cell growth [13]. However, this discrepancy may come from differences in the experimental conditions such as the substrate stiffness and the nature of the cells. For instance, once ADSCs reach confluent, cell-cell interactions may trigger signals for differentiation [24]. It would be interesting to study ADSCs differentiation on these patterned surfaces.

Expression of lineage markers

ADSCs have been demonstrated to differentiate into multiple lineages, such as smooth muscle cells, chondrocytes, osteoblasts, and adipocytes [3–6]. To assess cell differentiation, qRT-PCR was conducted to compare the expression of differentiation markers, namely, SM22 for smooth muscle cells, Sox9 for chondrocytes, Runx2 for osteoblasts, and PPAR for adipocytes. The result of each experiment was determined by the normalization to its internal control (GAPDH), followed by the normalization to the corresponding ST experiment. As shown in Fig. 5, no significant difference in the adipocyte lineage marker PPAR was detected across the 3 patterns. This may be due to the high stiffness of glass

surface not being suitable for adipogenesis. As demonstrated in previous reports, higher cellular stress induced by ECM stiffness and cell-cell interactions could induce chondrogenesis and osteogenesis [12, 23]. Therefore, we assessed the progression towards these two lineages for ADSCs in different patterns, which led to different relative stresses. As shown in Fig. 5, the chondrogenic marker Sox9 was significantly up-regulated in the SF pattern relative to the ST pattern. Sox9 expression in the AF pattern also showed a higher value, but it had limited statistical significance. The osteogenic marker Runx2 expression was significantly elevated in the SF pattern relative to both AF and ST patterns. Again, the slightly higher expression of Runx2 in AF pattern than ST pattern lacks statistical significance. Assessment of myogenesis using the marker SM22a showed a different trend (Fig. 5). The SM22 expression in ST pattern was significantly elevated compared to AF pattern, however, the difference between SF and ST patterns was not significant. Given the fact that different levels of cellular alignment were seen in the three patterns, this trend may indicate a significant role of uniaxial alignment in myogenesis. The perfect uniaxial alignment in ST pattern may promote myogenic marker expression. When we compared AF and SF patterns, which shared similar levels of overall relative stress, the further disruption of cellular alignment in AF patterns seemed to reduce significantly the myogenic marker expression.

To further investigate ADSC differentiation, immunofluorescent staining was performed to verify the lineage markers expression at the protein level. Acquisition parameters were held constant during imaging to enable comparisons between immunostaining images. Representative images of corresponding differentiation markers from each pattern group were listed in Fig. 6, except PPAR due to the extremely low expression below the detection limit. To further verify the interesting trend in myogenesis, another early-stage myogenic marker SMA was also used. In good agreement with the qRT-PCR results, SM22 immunostaining appeared to be more intense, on average, in the ST and SF patterns vs. the AF pattern. Interestingly, the SMA staining showed relatively higher intensity in ST pattern compared to AF pattern and even SF pattern; this may further support the preference of uniaxial alignment in myogenesis. In Runx2 and Sox9 stainings, the immunostaining results agreed with the qRT-PCR results, with staining being more intense in SF pattern compared to AF and ST patterns. Combining both the qRT-PCR and the immunostaining results, it appears that the increased relative stress induced by geometric cues could facilitate chondrogenic and osteogenic lineage progression. In contrast, the uniaxial cell alignment can promote expression of myogenic markers, and the alignment might be a more important factor for myogenesis than high peak stress. This finding is consistent with the observation in mouse multipotent cells [17].

Conclusions

In this study, we used a DOPsL biofabrication system to create multicellular forms to study the ADSC differentiation. The biological blank-slate property of PEGDA was utilized to create walls to confine the cells to form multicellular forms. Compared to normal patterning methods, such as micro-contact printing, which created cell adhesion islands, our wall design can prevent cell migration between patterns and thus facilitate the maintenance of the cell patterns with small gaps between patterns (e.g. <20um). This compact pattern can accommodate large number of cells in a small area to achieve highly efficient, cost-effective, and user-friendly operation to perform quantitative analyses, such as qRT-PCR and western blot. In addition, it is also feasible to study the cross-talk between patterns, such as paracrine signals, between the small gaps.

Our approach allows the studies of the roles of uniaxial alignment and form-induced stress on ADSCs differentiation. Under our experimental conditions, increased cell-substrate stress

tended to promote early-stage chondrogenic and osteogenic markers expression, and uniaxial alignment appeared to be more inductive of myogenic lineage progression in comparison to the patterns with higher stress but randomized cellular directionality. All the differentiation studies were performed in normal growth media without addition of extra growth factors. These findings could potentially contribute to the rational design of scaffolds for tissue engineering applications.

Supplementary Material

Refer to Web version on PubMed Central for supplementary material.

Acknowledgments

References

[1]. Berthiaume F, Maguire TJ, Yarmush ML. Tissue engineering and regenerative medicine: history, progress, and challenges. Annu Rev Chem Biomol Eng. 2011; 2:403–30. [PubMed: 22432625]

[2]. Safford KM, Hicok KC, Safford SD, Halvorsen YD, Wilkison WO, Gimble JM, et al. Neurogenic differentiation of murine and human adipose-derived stromal cells. Biochem Biophys Res Commun. 2002; 294(2):371–9. [PubMed: 12051722]

[3]. Erickson GR, Gimble JM, Franklin DM, Rice HE, Awad H, Guilak F. Chondrogenic potential of adipose tissue-derived stromal cells in vitro and in vivo. Biochem Biophys Res Commun. 2002; 290(2):763–9. [PubMed: 11785965]

[4]. Halvorsen YD, Franklin D, Bond AL, Hitt DC, Auchter C, Boskey AL, et al. Extracellular matrix mineralization and osteoblast gene expression by human adipose tissue-derived stromal cells. Tissue Eng. 2001; 7(6):729–41. [PubMed: 11749730]

[5]. Mizuno H, Zuk PA, Zhu M, Lorenz HP, Benhaim P, Hedrick MH. Myogenic differentiation by human processed lipoaspirate cells. Plast Reconstr Surg. 2002; 109(1):199–209. [PubMed: 11786812]

[6]. Zuk PA, Zhu M, Mizuno H, Huang J, Futrell JW, Katz AJ, et al. Multilineage cells from human adipose tissue: implications for cell-based therapies. Tissue Eng. 2001; 7(2):211–28. [PubMed: 11304456]

[7]. Gimble JM, Katz AJ, Bunnell BA. Adipose-derived stem cells for regenerative medicine. Circ Res. 2007; 100(9):1249–60. [PubMed: 17495232]

[8]. Konno M, Hamabe A, Hasegawa S, Ogawa H, Fukusumi T, Nishikawa S, et al. Adipose-derived mesenchymal stem cells and regenerative medicine. Dev Growth Differ. 2013; 55(3):309–18. [PubMed: 23452121]

[9]. Mizuno H, Tobita M, Uysal AC. Concise review: Adipose-derived stem cells as a novel tool for future regenerative medicine. Stem cells. 2012; 30(5):804–10. [PubMed: 22415904]

[10]. Wozniak MA, Chen CS. Mechanotransduction in development: a growing role for contractility. Nat Rev Mol Cell Biol. 2009; 10(1):34–43. [PubMed: 19197330]

[11]. McBeath R, Pirone DM, Nelson CM, Bhadriraju K, Chen CS. Cell shape, cytoskeletal tension, and RhoA regulate stem cell lineage commitment. Dev Cell. 2004; 6(4):483–95. [PubMed: 15068789]

[12]. Engler AJ, Sen S, Sweeney HL, Discher DE. Matrix elasticity directs stem cell lineage specification. Cell. 2006; 126(4):677–89. [PubMed: 16923388]

[13]. Nelson CM, Jean RP, Tan JL, Liu WF, Sniadecki NJ, Spector AA, et al. Emergent patterns of growth controlled by multicellular form and mechanics. Proc Natl Acad Sci U S A. 2005; 102(33):11594–9. [PubMed: 16049098]

[14]. Gao L, McBeath R, Chen CS. Stem Cell Shape Regulates a Chondrogenic Versus Myogenic Fate Through Rac1 and N-Cadherin. Stem cells. 2010; 28(3):564–72. [PubMed: 20082286]

[15]. Kilian KA, Bugarija B, Lahn BT, Mrksich M. Geometric cues for directing the differentiation of mesenchymal stem cells. Proc Natl Acad Sci U S A. 2010; 107(11):4872–7. [PubMed: 20194780]

[16]. Dang JM, Leong KW. Myogenic Induction of Aligned Mesenchymal Stem Cell Sheets by Culture on Thermally Responsive Electrospun Nanofibers. Adv Mater. 2007; 19(19):2775–9. [PubMed: 18584057]

[17]. Munoz-Pinto DJ, Qu X, Bansal L, Hayenga HN, Hahn J, Hahn MS. Relative impact of form-induced stress vs. uniaxial alignment on multipotent stem cell myogenesis. Acta Biomater. 2012; 8(11):3974–81. [PubMed: 22796654]

[18]. Zhang AP, Qu X, Soman P, Hribar KC, Lee JW, Chen S, et al. Rapid fabrication of complex 3D extracellular microenvironments by dynamic optical projection stereolithography. Adv Mater. 2012; 24(31):4266–70. [PubMed: 22786787]

[19]. Lu Y, Mapili G, Suhali G, Chen S, Roy K. A digital micro-mirror device-based system for the microfabrication of complex, spatially patterned tissue engineering scaffolds. J Biomed Mater Res A. 2006; 77(2):396–405. [PubMed: 16444679]

[20]. Soman P, Chung PH, Zhang AP, Chen S. Digital Microfabrication of User-Defined 3D Microstructures in Cell-Laden Hydrogels. Biotechnol Bioeng. 2013 doi: 10.1002/bit.24957.

[21]. Fairbanks BD, Schwartz MP, Bowman CN, Anseth KS. Photoinitiated polymerization of PEG-diacrylate with lithium phenyl-2,4,6-trimethylbenzoylphosphinate: polymerization rate and cytocompatibility. Biomaterials. 2009; 30(35):6702–7. [PubMed: 19783300]

[22]. Xu F, Beyazoglu T, Hefner E, Gurkan UA, Demirci U. Automated and adaptable quantification of cellular alignment from microscopic images for tissue engineering applications. Tissue Eng Part C Methods. 2011; 17(6):641–9. [PubMed: 21370940]

[23]. Ruiz SA, Chen CS. Emergence of Patterned Stem Cell Differentiation Within Multicellular Structures. Stem cells. 2008; 26(11):2921–7. [PubMed: 18703661]

[24]. Yoon HH, Bhang SH, Shin JY, Shin J, Kim BS. Enhanced cartilage formation via three-dimensional cell engineering of human adipose-derived stem cells. Tissue Eng Part A. 2012; 18(19–20):1949–56. [PubMed: 22881427]
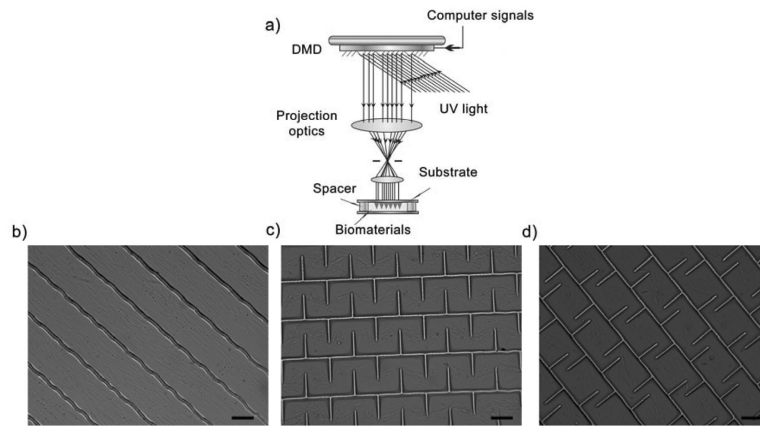
Figure 1.
Schematic view of the DOPsL system and fabricated structures. a) Schematic view of the DOPsL fabrication platform. b–d) DIC images of ADSCs seeded on patterned structures with 20% PEGDA. b) Stripes pattern (ST), c) symmetric fork pattern (SF), d) asymmetric fork pattern (AF). Scale bars are 100μm.
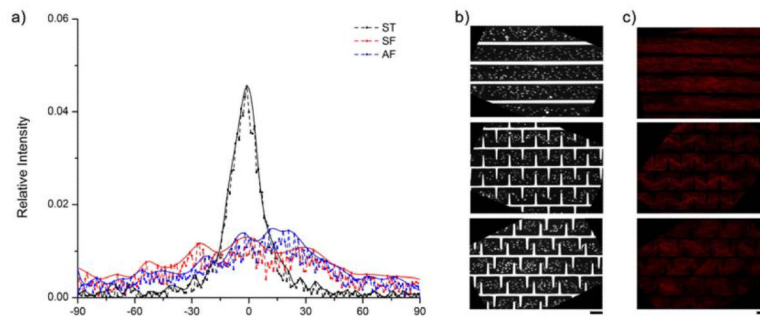
Figure 2.
Quantification of the cellular alignment induced by the patterns. a) Histogram showing alignment distribution of cells in stripes (ST), symmetric fork (SF), and asymmetric fork (AF) patterns. b) Representative binarized images of nuclear staining of cells in three patterns for alignment analysis. c) Representative fluorescent images of F-actin staining of cells in three multi-cellular forms. Scale bars are 100μm.
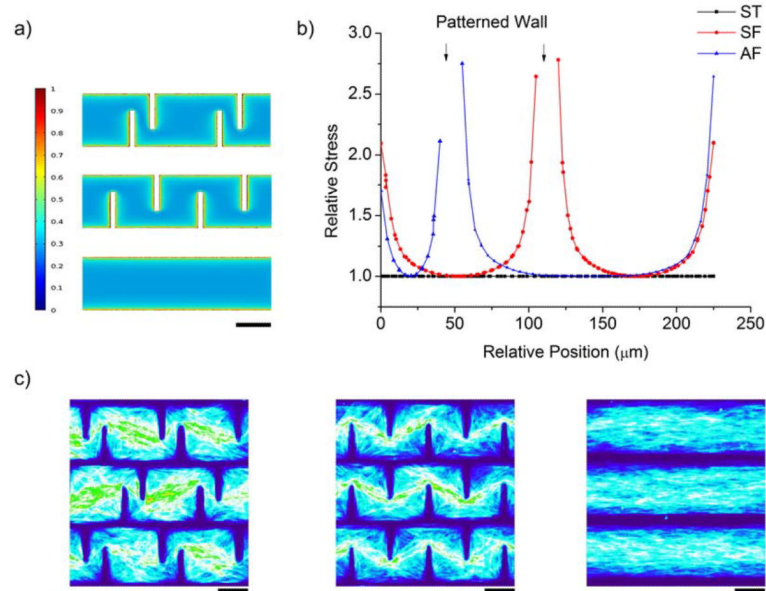
Figure 3.
Evaluation of relative cell-substrate stresses within the patterns. a) Finite element modeling results of the stress distributions within the three patterns. b) Plot of relative stress across the center of the patterns calculated in the FEM analysis. c) Heat map generated in FIJI software using stacks of F-actin staining images to show cellular distribution. Scale bars are 100μm.
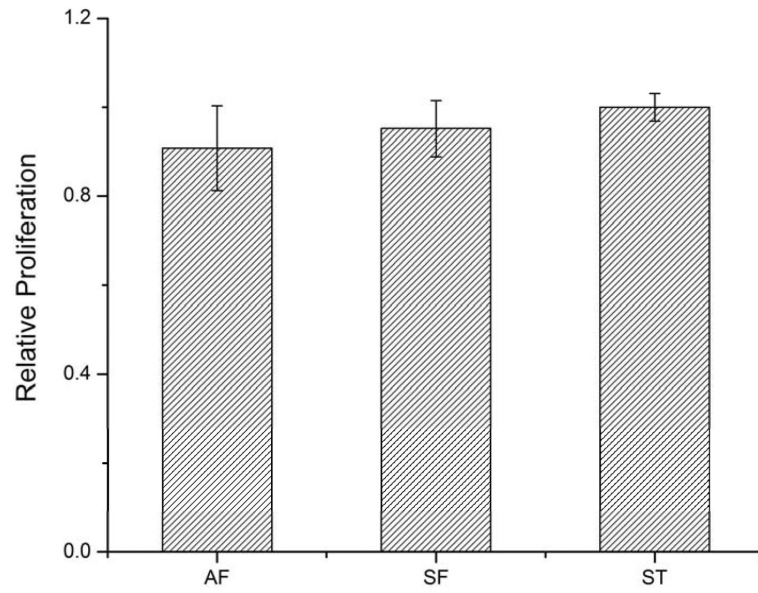
Figure 4.
Comparison of relative proliferation in three patterns showed no significant difference across groups.
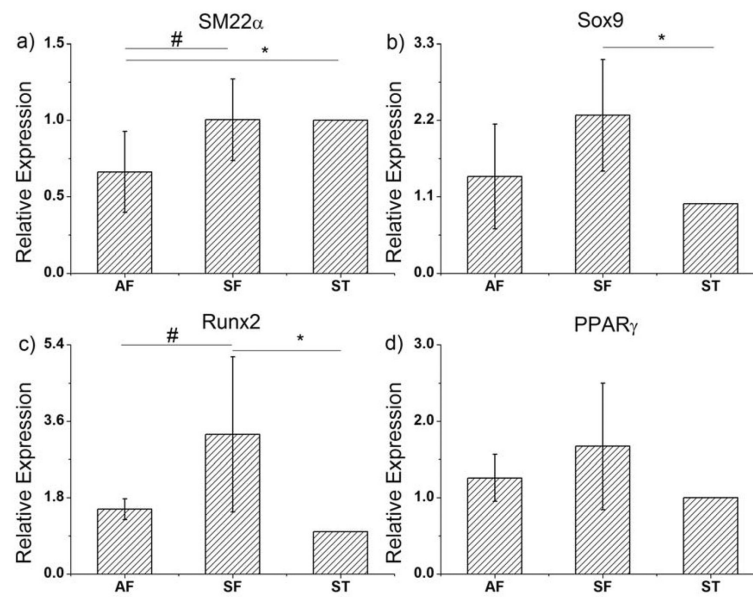
Figure 5.
qRT-PCR for Quantification of ADSC differentiation within different multicellular forms. Relative expression of differentiation markers in asymmetric (AF) and symmetric forks (SF) were compared relative to stripes pattern (ST). # indicates significant difference between AF and SF patterns, p<0.05. * indicates significant difference between AF or SF and ST patterns, p<0.05. a) SM22 expression, b) Chondrogenic marker Sox9 expression. c) Osteogenic marker Runx2 expression. d) Adipose lineage marker PPAR expression.
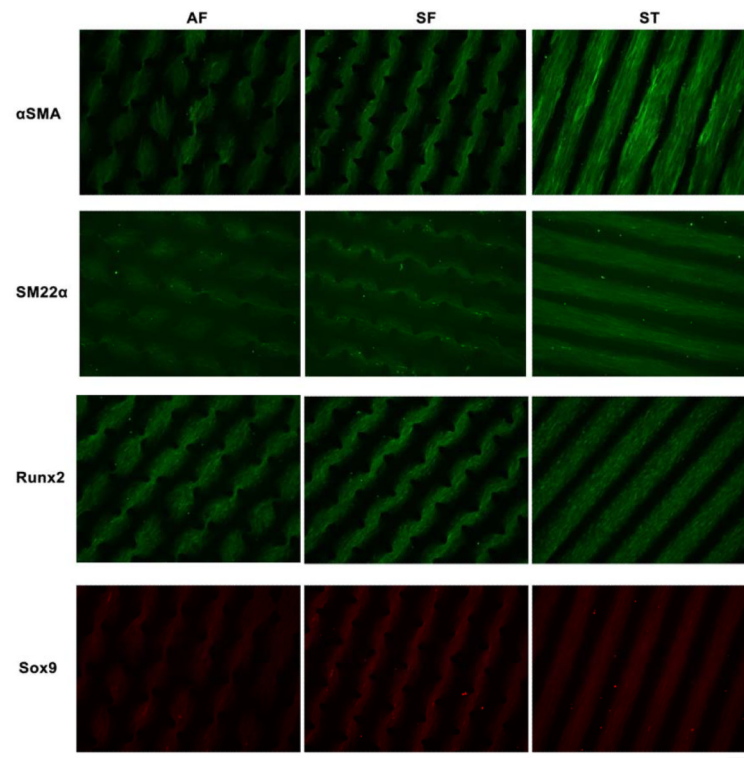
Figure 6.
Immunofluorescent staining of differentiation markers in three patterns showed trends consistent with those obtained by qRT-PCR. The images show higher expressions of SMA and SM22 in ST pattern relative to SF and AF patterns, and higher levels of Runx2 and Sox9 in SF pattern compared to the other two patterns. Scale bar is 200μm.